Cement 12 (2023) 100070

Contents lists available at ScienceDirect

Cement

journal homepage: www.sciencedirect.com/journal/cement

Effect of fluorite addition on the reactivity of a calcined treated spent pot lining in cementitious materials

Victor Brial [a], Hang Tran [b], Luca Sorelli [b], David Conciatori [b], Claudiane M. Ouellet-Plamondon [a,*]

[a] Department of Construction Engineering, École de Technologie Supérieure, Université du Québec, Canada
[b] Department of Civil and Water Engineering, Université Laval, Canada

ARTICLE INFO

Keywords:
Low caustic leaching liming
Treated spent pot lining
Blended cement
Hazardous waste
Aluminum
Supplementary cementitious materials

ABSTRACT

Treating SPL by the low caustic leaching and liming process generates an inert nonhazardous residue called LCLL Ash and a fluorite byproduct Calcined LCLL Ash that is ground into a fine powder demonstrates pozzolanic behavior in cement. The effect of the calcination temperature and fluorite byproduct addition on the reactivity of LCLL Ash was studied by the compressive strength activity index, Frattini test and Rilem R^3 tests followed by XRD analysis. At 800°C, the formation of nepheline causes alkali uptake, the LCLL Ash showed a slightly lower reactivity with 10% fluorite addition. At 1000°C, calcined LCLL Ash/CF showed a better amorphization of phases and increasing reactivity due to reactions between fluorite and sodium oxide. Unlike LCLL Ash, no delay in hydration or hydro reactivity was observed with calcined LCLL Ash/CF.

Introduction

Cement is the largest manufactured product on Earth by mass. The cement industry is a major emitter of greenhouse gases and is responsible for approximately 5-8% of global CO_2 emissions [1,2]. With the aim of many countries to reach carbon neutrality by 2050, reducing greenhouse gas emissions from this industry is inevitable. Due to the industry's high energy consumption, the cement manufacturing process has already been optimized for economic and environmental reasons (for example, using a dry process and precalciner) [3–6]. However, emissions from the manufacturing process represent only approximately 40% of emissions. The remaining 60% cannot be reduced because they are a result of calcite decarbonation [3,7]. One of the best options for reducing the carbon footprint of concrete is the use of supplementary cementitious materials (SCMs) or fillers to replace part of the cement in the concrete [6]. SCMs are mostly byproducts or residual materials from other industries, such as silica fume or granulated blast furnace slag (GBFS). However, apart from calcined clays and fillers, the availability of SCMs remains quite limited due to logistics, chemical and mineralogical composition, contamination, or even local availability constraints [6]. This is particularly the case in Quebec, Canada, which does not have locally produced GBFS, kaolin or fly ash since electricity is produced by hydraulics.

Thanks to the high availability of hydroelectricity, Quebec is a major producer of primary aluminum, with a production volume of 2.47 million tons in 2018 [8]. The production of primary aluminum in electrolytic tanks generates hazardous wastes that are subsequently treated but are not currently preventable. Among these residual materials is the spent pot lining (SPL), which results from the end of life of the cathode and the refractory of the electrolytic cells. SPL is a hazardous material due to its leachable fluoride and cyanide, as well as its hydro reactivity, which results in the generation of explosive gases [9–11]. Therefore, SPL must be treated before disposal in a landfill. Different solutions are currently used to treat or upgrade SPL. Before its treatment, the SPL can, if necessary, be separated into two parts: the first cut is rich in carbon materials from the cathode, and the second cut is rich in vitrified refractory material. SPLs can be treated by pyro-metallurgical or hydro-metallurgical means [12]. However, the majority of pyrometallurgical treatment processes have been abandoned, leaving only two hydro-metallurgical processes [13].

Developed in the 1990s, the low caustic leaching and liming (LCL&L) process is one of only two hydrometallurgical treatment methods for SPL treatment [9,14]. As shown in the diagram in Fig. 1, the SPL is ground and then water leached in a low caustic solution to neutralize the hydro reactivity and add fluorides and cyanides into the solution. The solid part is then filtered out to obtain an inert residue. The treatment of the

* Corresponding author at: École de technologie supérieure, 1100, rue Notre-Dame Ouest, Montréal (Québec) Canada H3C 1K3.
E-mail address: claudiane.ouellet-plamondon@etsmtl.ca (C.M. Ouellet-Plamondon).

https://doi.org/10.1016/j.cement.2023.100070
Received 6 November 2022; Received in revised form 6 April 2023; Accepted 11 April 2023
Available online 14 April 2023

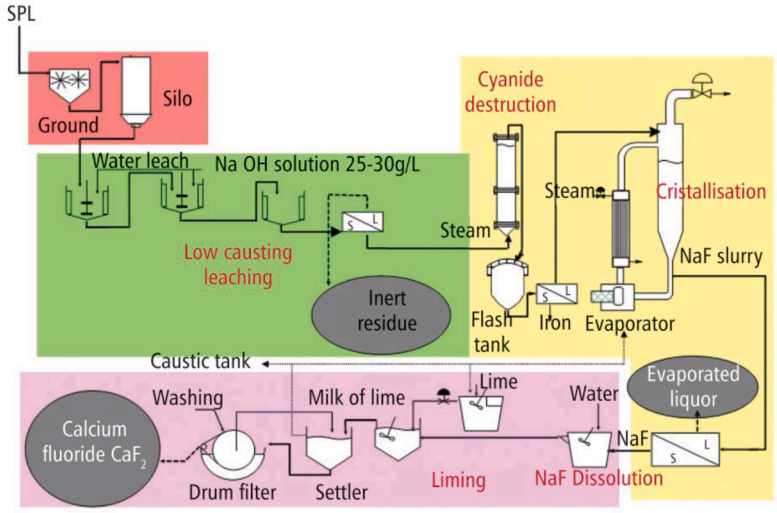

Fig. 1. LCL&L process diagram from Birry et al. [14].

second cut after this water leaching stage allows us to obtain a residue rich in silica, alumina, iron oxide and sodium called LCLL Ash. The recovered solution is then treated at high temperature and pressure to destroy the cyanides. The remaining NaF-rich solution is then evaporated to obtain solid NaF. The NaF is then mixed with a lime solution to transform the NaF into fluorite and regenerate the caustic solution. Following this operation, a calcium fluoride byproduct (CF) with a content of approximately 85% fluorite is obtained. This CF is then mostly recovered to produce AlF_3, which will be reused in the electrolysis smelters as a bath additive [14]. Currently, the only facility treating SPLs using the LCL&L process is in Jonquière, Quebec.

Different solutions have been studied to valorize SPLs in the cement industry. In the 1990s, trials were carried out in France to mix untreated SPLs with raw meal from a cement plant [15]. The high clinkerization temperature destroys the cyanides, and the high concentration of calcium and silica uptakes the fluorine. The use of SPLs in the kiln reduces the consumption of fossil fuels by up to 4% and reduces the overall CO_2 emissions by 1%. These decreases in energy and emissions are due to a decrease in the clinkerization temperature of 20 to 100°C according to the SPL replacement percentage [16,17]. However, the replacement of raw meal with SPL material must be limited to between 0.2% and 0.75% to avoid durability concerns caused by alkali-silica reactions attributed to the high sodium content of SPLs [10,16–18].

This article is the third part of a global project studying the potential of treated SPL by LCL&L process as cementitious materials. The use of the second cut SPL treated by the LCL&L process, called LCLL Ash, in cement production has also been studied in the first part of this project [19,20]. LCLL Ash showed filler behavior with a retarding effect due to the presence of soluble alkalis. However, after calcination at 1000°C, LCLL Ash exhibited pozzolanic behavior similar to that of fly ash. Calcined LCLL Ash also exhibited phase changes in the hydration products. Due to its high content of available alumina, LCLL Ash precipitated more carboaluminate phases [19]. The calcination of materials at high temperature entails the consumption of important quantities of energy. The calcium fluorite is known to act as a flux agent to decreases the melting temperature in SiO_2-Al_2O_3 systems [21–24]. By calcinating LCLL Ash with calcium fluorite from the SPL treatment process, it may be possible to reduce the calcination temperature of LCLL Ash, or to increase it reactivity of calcined LCLL Ash in cement.

Calcining mineral products to improve their performance in cement is a common method used to improve clays or shales [3,25]. However, this method may seem counterintuitive because of its energy demand. Nevertheless, the calcination temperatures of clay shales are much lower than the clinkerization temperature of cement. In addition, most of the CO_2 emissions from cement result from the decarbonation of calcite. Replacing a part of the clinker with a material calcined at a lower temperature and without decarbonation leads to a reduction in the carbon footprint of this blended cement [26,27].

The objective of this article (third part of the project) is to demonstrate the potential of the circular economy by using residual materials (LCLL Ash and CF) from the aluminum industry as additives in the cement industry. This could possibly avoid landfilling and reduce the carbon impact of blended cement with calcined LCLL-ash/CF. This article aims to study and understand the effect of the addition of fluorite on the reactivity of LCLL Ash calcined at 800°C and 1000°C. The following questions will be answered:

(i) How do fluorite addition and calcination improve the reactivity of LCLL Ash?
(ii) What is the mechanism for the changes in the properties of the ash when co-calcined with calcium fluorite?
(iii) What is the optimum fluorite content to improve the reactivity of LCLL Ash after calcination at 800°C and 1000°C?

To answer these questions, the effect of the addition of fluorite on the mineralogy of the LCLL Ash/CF mixture after calcination at 800°C and 1000°C was evaluated. For each percentage of added fluorite tested, the mineralogical composition was analyzed by quantitative XRD Rietveld analysis to determine the phase changes. Then, the reactivity of the calcined LCLL Ash/CF mixtures was studied using the same methodology of Brial et al [19] with Frattini, mortar compressive strength, R^3 test and quantitative X-ray diffraction.

Materials and methods

Materials

The LCLL Ash and CF were obtained from the Rio Tinto treatment plant based in Jonquière, QC, Canada. Portland cement (Type GU, Ciment Québec, St Basile, QC, Canada) was used to prepare the Frattini and mortar samples. The calcined LCLL Ash/CF reactivity was compared to that of a quartz powder reference, named Q, that was made by grinding graded Ottawa sand. The Ottawa sand was ground with a Fritsch Pulverisette 9 vibrating cup mill in 100 g batches for 2 minutes at a speed of 1000 rpm.

The chemical compositions of the cement, LCLL Ash, fluorite byproduct (CF) and quartz powder were measured by X-ray fluorescence (XRF) after loss of ignition. The chemical compositions of Portland

Table 1
Chemical compositions of the cement and materials tested.

	Percentage in weight (wt%)											
Oxide	SiO_2	Al_2O_3	Fe_2O_3	CaO	MgO	SO_3	K_2O	Na_2O	TiO_2	P_2O_5	F	LOI
OPC	19.17	4.69	3.61	61.52	2.4	3.98	1.06	0.25	0.25	0.14	0.05	2.62
LCLL Ash	37.18	36.29	7.36	3.04	0.38	0.06	0.77	8.23	0.75	0.12	0.63	5.72
CF	-	0.64	-	98.8	-	0.5	-	-	-	-	65.6	4.62
Q	91.4	4.94	1.72	0.55	0.04	0	0.1	1.09	0.1	0.01	0.01	0

Table 2
Major mineralogical compositions of the OPC, LCLL Ash and quartz powder.

Phase	OPC	LCLL Ash	CF	Q
C_3S	63.2	-	-	-
C_2S	7.6	-	-	-
C_3A	3.7	-	-	-
C_4AF	11.9	-	-	-
Quartz	0.1	10.9	-	97.8
Corundum	-	14.2	-	-
Albite	-	9.1	-	-
Nepheline	-	21.4	-	-
Anorthite	-	11.6	-	1.8
Graphite	-	6.2	-	-
Mullite	-	3.7	-	-
Hematite	-	2.9	-	-
Magnetite	-	4.7	-	-
Fluorite		1.8	86.9	
β-Alumina		6.8		
Calcite	2.5	-	7.6	-
Anhydrite	-		0.6	-
Amorphous	-	5.8	-	-

cement, LCLL Ash, CF, and quartz powder are shown in Table 1. The composition of LCLL Ash is similar to a low calcium fly ash or a calcined clay with an important silica and alumina content. However, LCLL Ash shows a higher alkali content than clay or fly ash, as approximately 8% of its weight is sodium oxide. The CF composition is found by considering together the results for 98.8% calcium oxide, 65.6% of fluoride, in addition to traces of sulfate and aluminate. However, this concentration of calcium oxide cannot reflect its real proportion as it is overestimated due to accounting for the calcium in the calcium oxide form, and not as the CaF_2 form. In consequence, this CaO content is incorrect, as oxygen is not found within CaF_2.

The mineral phase compositions of the materials were measured by X-ray powder diffraction (XRD) and Rietveld analysis. The amorphous content was determined with a zincite (ZnO) external standard. The quantitative mineralogical compositions of the cement, the LCLL Ash, CF and quartz powder are presented in Table 2.

The LCLL Ash is mainly composed of crystalline phases, such as corundum, albite, nepheline, quartz and anorthite, in addition to the lower content of amorphous phases. As previously studied in [19,20], because of the high content of crystalline phases in LCLL Ash, it displays a behavior similar to that of fillers in cement. An additional calcination treatment is then necessary to increase the LCLL Ash reactivity. In addition, XRD results showed that the alkalis of LCLL Ash are present as alkaline plagioclase like albite. These phases have the advantage of being insoluble like quartz [28,29].

Methods

Calcined LCLL Ash/CF preparation

A 100 g mix of raw LCLL Ash and CF powder was initially ground in a Fritsch Pulverisette 9 vibrating cup mill for 2 min 30 s at a speed of 1000. The added CF content was tested with a replacement of LCLL Ash from 0% to 20% with 2.5% increments for XRD analysis. Otherwise, all remaining tests were carried out with 0%, 5%, 10%, 15%, and 20% CF replacement. The samples were named in the form X LCLL Y CF Z, where X, Y and Z refer to the percentage of LCLL Ash, the percentage of CF and the calcination temperature, respectively. For each mix, 3 samples of 200 g ground LCLL Ash/CF were calcined for 2 h in a high-temperature Nabertherm N11/H furnace at 800°C to 1000°C. The calcination

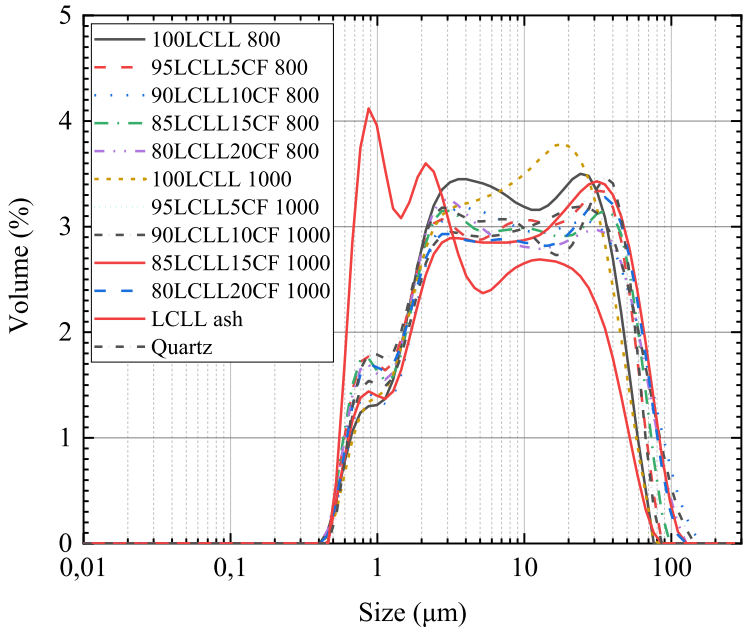

Fig. 2. Particle size analysis by laser granulometry.

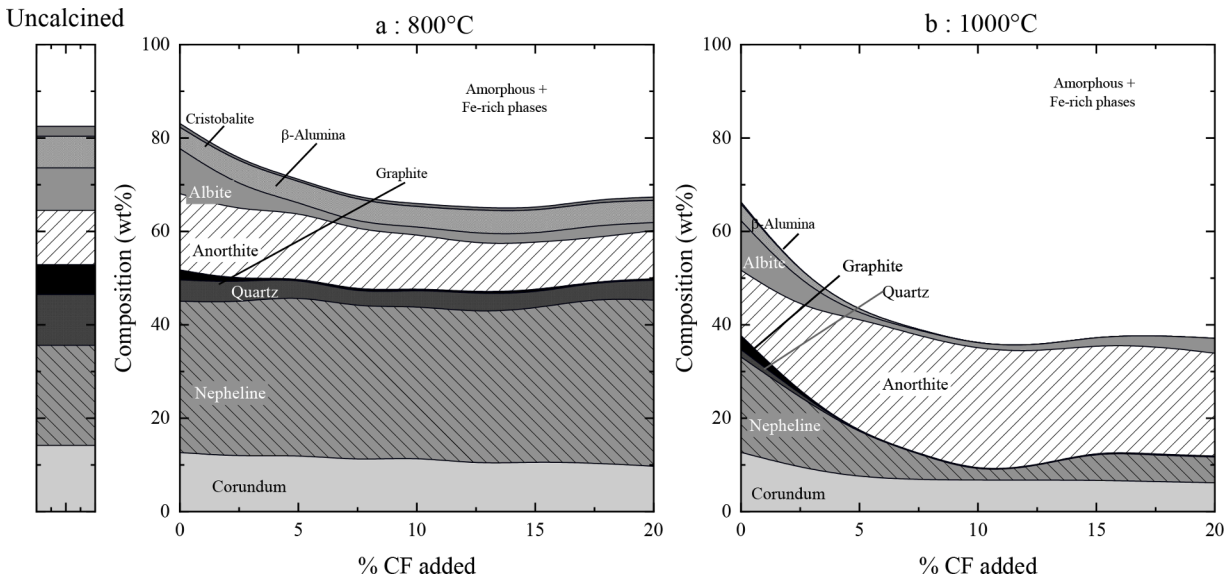

Fig. 3. XRD quantitative analysis of calcined LCLL Ash after cooling a) at 800°C and b) at 1000°C. The CF concentration was removed to a better understanding

temperatures were selected according to Brial et al. [30] who identified two optimal temperature calcination of LCLL Ash of 800°C to 1000°C. The samples were removed from the furnace at high temperature and cooled by air quenching on a metallic plate until they reached room temperature. The calcined LCLL Ash/CF obtained from the 3 crucibles were mixed together and ground with the same vibrating cup grinder for 20 s and 90 s for the mixes calcined at 800°C and 1000°C, respectively. The objective of the second grinding was to obtain the same d_{50} of approximately 10 ± 5 μm to limit the effect of the granulometry. Each calcined LCLL Ash/CF mix was analyzed using a Malvern Mastersizer 3000 by laser diffraction granulometry using isopropanol as dispersant to measure the particle size distribution (PSD). The results of the particle size distribution of the calcined mix is presented in Fig. 2.

Mortar

The reactivity of the mixes was first analyzed by measuring the compressive strength of the mortar with a replacement of 20% of the cement by calcined LCLL Ash/CF and a water/binder ration of 0.485. The mortar was prepared according to the ASTM C109 [31] standard and with the same method as Brial et al [19]. Mortar mixes were tested at 1, 7, 28 and 112 days.

Frattini test

To characterize the pozzolanic reactivity of the calcined LCLL Ash/CF mixes. Frattini tests were carried out. This test determined the pozzolanic reactivity of SCMs by evaluating calcium consumption by comparing the calcium concentration to the lime solubility curve [32] for a given concentration of hydroxyl ions. Frattini test is one of the most common used tests in literature to evaluate the reactivity of SCMs. However, this test can only detect pozzolanic materials but no hydraulic or latent hydraulic materials [33,34]. Samples were prepared by mixing 16 g of Portland cement and 4 g of SCM with 100 ml of distilled water. The samples were left in sealed plastic bottle and placed in an oven at 40°C for 8 days. The sample was analyzed with the same method as Brial et al. [19] by measuring the concentration of calcium and hydroxyl ions respectively by ICP-OES and titration after filtration with a 0.2 μm syringe filter. In addition, the concentrations of Al, Na, K, and Si in the supernatant solution were also measured by ICP–OES. For more details on the method, refer to Brial et al [19].

R3: Heat release and portlandite consumption

According to the recommendation of Donatello et al. [34], the Frattini tests should be used in combination of the independent method to characterize the real portlandite consumption by the reactive SCMs. To complement this article, R^3 tests were used. The R^3 methods were initially developed to study the reactivity of calcined clay in limestone calcined clay cement (LC^3). These methods can be extended to evaluate the reactivity of other SCMs. There are several R^3 tests to access SCM reactivity. As for Brial et al [19], this article analyzed the reactivity of tested SCMs by measuring the heat released and the portlandite consumption respectively measured by isothermal calorimetry and thermogravimetric analysis. The R^3 paste was obtained by mixing 33.33 g of calcium hydroxyl, 11.11 g of tested SCM, and 5.56 g calcium carbonate in a solution of 60 mL made of distilled water with 1.20 g of KOH and 0.24 g of K_2SO_4 [35]. This chemical composition of this paste allows to recreate the chemistry of limestone cement without cement phases. Isothermal calorimetry was carried out with a TA TamAir calorimeter to measure for 7 days the heat release by the R^3 paste at 40°C. For each calcined LCLL Ash/CF sample tested, the R^3 paste was mixed at 1600 rpm in a plastic tube, and 16 g of paste was introduced in a calorimetry ampoule. The portlandite consumption was measured by a Perkin Elmer STA8000 TGA analyzer following a hydration stoppage by solvent exchange. The R^3 testes were realized and analyzed according the same method as Brial et al [19]. For more information on the parameters used, refer to Brial et al [19].

X-ray diffraction

To identify the mineral phase transformations during calcination, mixes of calcined LCLL Ash/CF were analyzed by XRD. Moreover, to evaluate the influence of calcination temperature and fluorite replacement on the precipitated phases during the test, R^3 mixes were also analyzed by quantitative XRD. In both cases, data were collected on a Bruker D8 Advance diffractometer using Cu K-alpha radiation operated at 40 kV and 40 mA. The sampled were prepared by solvent exchange and analyzed by Rietveld analysis according to the same methods as Brial et al [19]. The amorphous content was determined with a zincite external standard corrected with the mass absorption coefficient. For more information about the parameters used to record XRD data, refer to Brial et al [19].

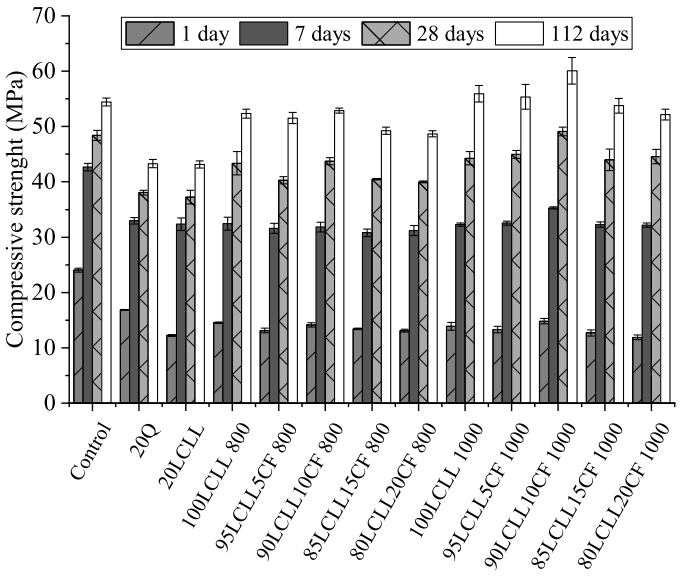

Fig. 4. Mortar compressive strength of with 20% calcined LCLL Ash replacement at 1, 7, 28 and 112 days (mean values and standard deviation bars).

Results

Calcined LCLL Ash/fluorite composition

Fig. 3a and b show the compositions of the calcined LCLL Ash/CF samples at 800°C and 1000°C, respectively, as a function of CF addition. The mineralogical composition was measured by quantitative XRD analysis after cooling and grinding. However, iron-rich phases were counted with the amorphous content due to technical difficulties in observing and quantifying these phases by XRD.

Due to its composition, the main reactions at high temperature will take place between the three main oxides SiO_2, Al_2O_3, and Na_2O according to the following equations:

$$Na_2O + Al_2O_3 + 6\ SiO_2 = 2\ NaAlSi_3O_8\ (\text{Albite}) \quad (1)$$

$$NaAlSi_3O_8 + Al_2O_3 + Na_2O = 3\ NaAlSiO_4\ (\text{Nepheline}) \quad (2)$$

$$2\ NaAlSiO_4 + 4\ SiO_2 = 2\ NaAlSi_3O_8 \quad (3)$$

The calcination of LCLL Ash at 800°C without the addition of fluorite showed significant changes in the mineralogy with an increase in the amount of amorphous material from 5% to 20%. In addition, great increases in nepheline and anorthite are also observed, with concentrations increase from approximately 21% to 30% and from 12% to 16%, respectively. These increases are accompanied by decreases in the corundum, quartz and β-alumina contents of 4%, 6%, and 3%, respectively, which indicates the formation of albite and nepheline according to Eqs. 1 and 2. Similar results have been observed by Wang et al. [36] and Chen et al. [37] for a mixture containing 10% Na_2O.

The addition of CF will lead to the formation of a greater amorphous phase content. Similar observations were made by Wang et al. [21] and Zhang et al. [38]. This increase reached a maximum amorphous content between 19%, without adding CF, to 31% when the CF addition ranged between 10 and 12.5%. When the CF addition was more than 12.5%, the amorphous phase content decreased. The decrease observed here is due to the addition of CF, which decreases the concentration of LCLL Ash in the mixture and increases the concentration of fluorite. The addition of CF also greatly affects the concentration of albite, which is rich in silica, which decreases in concentration from 10% without CF addition to 2% with a CF replacement of 5% to 20%. In addition, the nepheline concentrations remain stable at approximately 30% despite the decrease in the concentration of LCLL Ash, which indicates an increase in nepheline formation upon the addition of CF. This increase is possibly attributed to the equilibrium between nepheline and albite according to Eqs. 2 and 3. On the other hand, the formation of anorthite and beta-alumina does not seem to be affected by the addition of CF.

Calcined at 1000°C, the LCLL Ash without the addition of CF shows a more important generation of amorphous content than the LCLL Ash calcined at 800°C, as an increase of 20% to 35%wt was observed. Calcination also shows significant changes in mineralogy, as a 10% decrease in nepheline concentration compared to calcination at 800°C was observed. This decrease is accompanied by an increase in the concentrations of albite, anorthite and corundum, with concentrations of 10.6%, 14.0% and 12.7%, respectively. A strong decrease in quartz and beta-alumina is also observable with respective decreases of 8% and 4%. Similar results were obtained by Wang et al. [36] and Chen et al. [37]. The addition of CF to the mixture calcined at 1000°C further increased the formation of amorphous material, which reached a maximum of 62% for CF additions of 10% and 12.5%. This maximum amorphous content is similar to the observations made for the mixture at 800°C. Beyond 12.5% CF, the dilution of LCLL Ash increases, which leads to a decrease in amorphous phase formation. With the addition of CF ranging from 0% to 10%, the concentrations of albite, nepheline, quartz, corundum and beta-alumina greatly decreased, which led to the creation of amorphous structures. However, the anorthite concentration reached a maximum level when an addition of 10% CF was used. At concentrations beyond 10%, anorthite remained the major phase. Moreover, the absence or low concentration of fluorite for additions of 0% to 10% CF seems to indicate that the fluorite reacted by providing CaO to the formation of anorthite according to Eq. 4 [39,40].

$$Na_2O + CaAl_2Si_2O_8\ (\text{Anorthite}) = 2\ NaAlSiO_4 + CaO \quad (4)$$

Mortar relative strength

The compressive strength and relative strength results of tested mixes are presented in Figs. 4 and 5, respectively. The replacement of 20% of cement by an inert material generates a dilution effect that is equivalent to a water/binder ratio increase from 0.485 to 0.610 causing a porosity increased and a compressive strength decreased [41,42]. According to Fig. 4, this effect is visible from 1 to 112 days the replacement of 20% quartz with a reduction of approximately 30 to 20% in compressive strength, respectively. LCLL Ash/CF mixes calcined at 800°C and 1000°C exhibit lower compressive strength than Portland cement and quartz mortars, with similar results to LCLL Ash at 1 day. At 7 days, all the mixes showed compressive strength's similar to that of quartz at approximately 32 MPa. However, the 90LCLL10CF mix calcined at 1000°C exhibits a higher compressive strength than quartz but a lower compressive strength than cement. After 28 days, all the calcined mixes reach compressive strengths between 40 MPa and 45 MPa, which are higher than quartz and LCLL Ash but lower than the Portland cement reference. Only 90LCLL10CF calcined at 1000°C showed a compressive strength similar to that of the OPC reference. The same trends were observed at 112 days. For each mix, the relative compressive strength (RCS) was calculated according to the following equation:

$$RCS = \frac{R^{i\ days}_{100\ cement} - R^{i\ days}_{20SCM}}{R^{i\ days}_{100\ cement}} \quad (5)$$

where $R^{i\ days}_{100\ Cement}$ and $R^{i\ days}_{20SCM}$ are the compressive strength of the cement reference at i-days and the blended cement with calcined LCLL Ash/CF or Q at i-days, respectively.

As shown in Fig. 5, the mortar mix containing quartz exhibits a decrease of approximately 20% to 30% in compressive strength for all days tested. Similar observations were made by [33,34,42] and confirm the dilution effect for inert materials. The relative 1-day strength of LCLL Ash is 10% lower than the value of quartz. However, similar results to

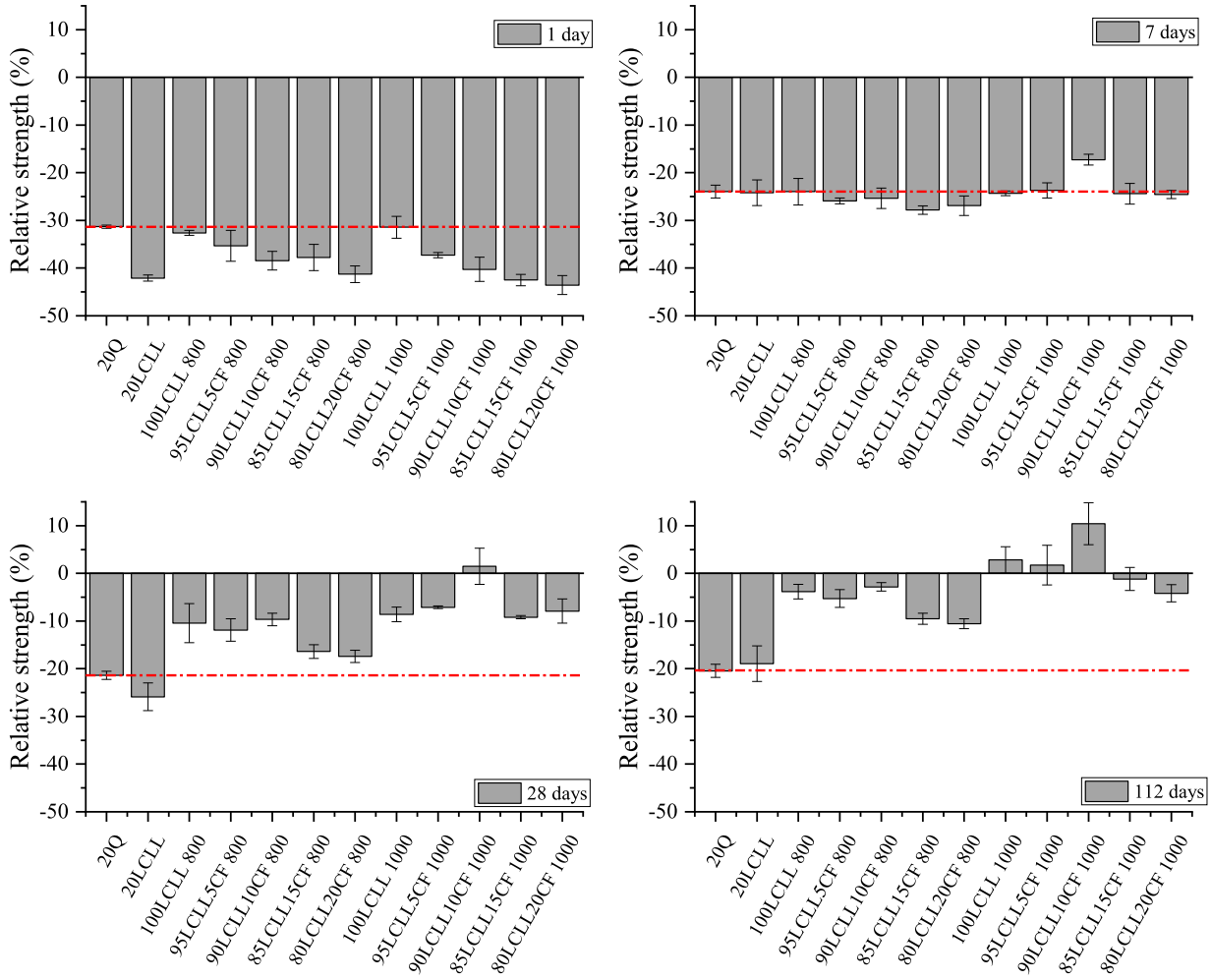

Fig. 5. Relative compressive strength values of mortar s with calcined LCLL Ash at 1, 7, 28 and 112 days. The red line illustrates the quarts reference mortar.

quartz were observed for LCLL Ash calcined at 800°C and 1000°C without CF addition. Similar results were observed by Brial et al. [19] for LCLL Ash calcined at 1050°C. The lower compressive strength results of LCLL Ash at 1 day translate a retarder effect of LCLL Ash in cement describe by Brial et al [19]. This retard can be explained by the high concentration of soluble alkalis [43] or the presence of carbonaceous material (graphite), comparable to fly ash [44,45]. However, the origin of this delay is currently not well understood. A longer delay is also observed for all mixes containing LCLL Ash/CF calcined at 800°C and 1000°C. The drop in compressive strength is proportional to the addition of CF. As this decrease is not observed in the mixtures of calcined LCLL Ash without CF, the addition of fluorite is responsible for this delay. Indeed, the research of Guo et al. [46] and Odler et al. [47] showed that the presence of F^- ions causes delays in the hydration of C_3S and C_3A.

At 7 days, the mix of LCLL Ash/CF calcined at 800°C exhibited a reduction of approximately 25% in relative compressive strength, similar to quartz. Mix 90LCLL10CF calcined at 1000°C showed slightly higher relative compressive strength values than the quartz reference, indicating a beginning of reactivity. For all the other mixes, values similar to quartz were observed. The calcined LCLL Ash and calcined LCLL Ash/CF mixes showed a decrease of approximately 10% in the relative compressive strength after 28 days. However, these values are higher than those of noncalcined LCLL Ash and quartz, which indicates the presence of reactive phases. The LCLL Ash/CF samples calcined at 800°C with CF additions of 15% and 20% showed a reduction in the relative compressive strength of 15%. These values are lower than those of LCLL Ash calcined at the same temperature. On the other hand, the mixture containing 10% CF calcined at 1000°C showed a resistance similar to that of the mortar containing 100% Portland cement. At 112 days, the LCLL Ash exhibits unreactive behavior with a compressive strength reduction similar to that of quartz. For the mixes calcined at 800°C, a slightly lower reduction in the compressive strength of approximately 5% was observed for mixes with 0%, 5%, and 10% CF. However, the mixes containing 15% and 20% CF showed lower results, with a reduction in compressive strength of approximately 15%. The mixes calcined at 1000°C showed results for CF additions from 0% to 10% similar to or higher than that of Portland cement. Nevertheless, a decrease in relative strength was observed for mixes calcined at 1000°C containing 15% and 20% CF. These results confirmed previous observations regarding the mineralogy of calcined LCLL Ash/CF, with an optimum reactivity reached at 10% replacement of LCLL Ash by CF. Moreover, LCLL Ash/CF calcined at 1000°C showed higher reactivity than mixes calcined at 800°C. Nevertheless, CF additions higher than 10% exhibit a decrease in compressive strength, indicating a lower reactivity.

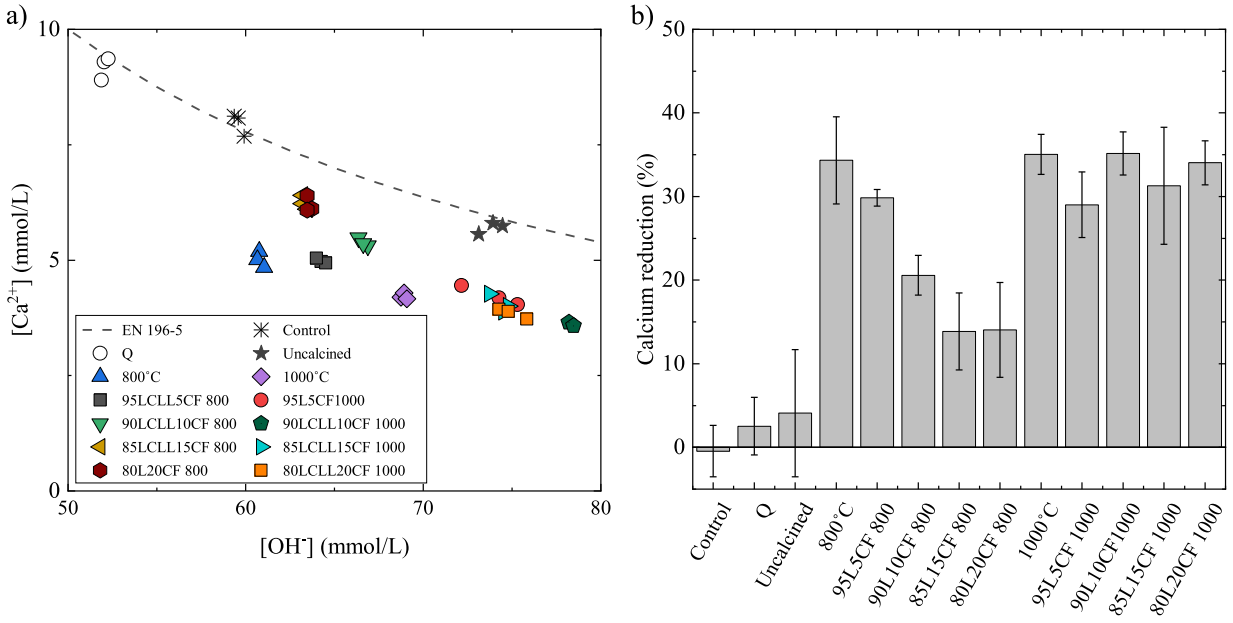

Fig. 6. a) Frattini results for the calcination temperatures tested. The dashed line refers to the max CaO content according to the EN-196-5 European standard and b) calcium reduction from the Frattini test for each calcination temperature tested.

Frattini tests

The results of the Frattini tests are presented Fig. 6a and b. These figures show the calcium concentration as a function of the OH^- ion concentration and the calcium reduction measured for LCLL Ash/CF mixes calcined at 800°C and 1000°C, respectively. As did in Brial et al [19], the lime solubility curve was given by the European standard EN 196-5 [32].

As shown in Fig. 6a and 6b, the results of the Portland cement reference, quartz powder, and LCLL Ash samples are close to the lime saturation curve. These results indicate an absence or low consumption of portlandite, which reflects an absence of pozzolanic reactivity. Similar results were observed by Brial et al. [19]. Calcination at 800°C allows a strong increase of approximately 35% in calcium reduction, indicating a strong increase in the pozzolanic reactivity of LCLL Ash calcined at 800°C. However, the addition of CF will cause a gradual decrease in calcium reduction, which will reach a minimum with mixtures containing 15% and 20% CF.

For mixes calcined at 1000°C, similar calcium reductions of approximately 30-35% were observed for all CF concentrations. These results confirm the pozzolanic behavior of the mixtures of LCLL Ash/CF calcined at 1000°C. However, no optimum percentage of CF was identified for the mixtures calcined at 1000°C according to this test. In addition, changes in the concentration of hydroxyl ions are observed with the evolution of the CF addition and the calcination temperature. Mixtures calcined at 1000°C show higher hydroxyl concentrations than mixtures calcined at 800°C. Despite this difference, the two calcination temperatures exhibit a similar trend of increasing hydroxyl concentration for the mixture with 10% CF, then a decrease for the mixtures with 15% and 20% CF additions.

The compositions of the solutions were also analyzed by ICP to determine the concentrations of K, Na, Al, and Si. The results of the ion concentration analysis are presented in Fig. 7. The K concentrations showed a lower value for the mixes with LCLL Ash or calcined LCLL Ash/CF. As cement is the main source of potassium, this potassium decrease is attributable to the replacement of 20% of the cement. The evolution of the hydroxyl ion concentration shows a similar trend to that of the sodium ion concentration. An increase in the sodium concentration is observable for the uncalcined LCLL mix. Similar trends were observed for the aluminum and silicon concentrations. The addition of non-calcined LCLL Ash causes a slight increase in Al and Si. Calcination at 800°C will increase the concentrations of available Al and Si. However, a greater increase is observable for the mixture with 5% CF. Finally, the mixes calcined at 1000°C showed higher concentrations of available Al and Si than the mixes calcined at 800°C. In particular, the aluminum concentrations were 2 to 3 times higher. In addition, the mix with 10% CF showed the highest Al and Si concentrations. These results confirm the better solubility and the reactivity increase with the calcination temperature but also for a CF addition of approximately 5 to 10%.

R^3: Heat release and calcium hydroxide consumption

The cumulative heat release results by R^3 paste are shown in Fig. 8a. The majority of the reactions of dissolution or hydration are exothermic; therefore, the analysis of the heat released allows to evaluate the presence of reactivity [3]. The heat measured mainly reflects the reaction of the material tested [48]. However, to improve the chemical kinetics, the R^3 test was carried out at 40°C. After 7 days, the quartz reference showed a weak heat release of approximately 25 J/g of SCM, which confirms its inert behavior [49].

Mixes calcined at 800°C showed lower concentrations, especially for mixes with 15% and 20% CF. However, higher concentrations are observable for mixtures calcined at 1000°C with values similar to uncalcined LCLL Ash at approximately 50 mmol/L. These results confirm the influence of the availability of sodium from LCLL Ash on the pH of the solution. A strong release of heat was observed for the uncalcined LCLL Ash with values of approximately 210 J/g of LCLL Ash. This result is surprising given the lack of reactivity observed during the tests on mortar and Frattini. However, signs of R^3 paste expansion were observed on each of the ampoules containing uncalcined LCLL Ash. As proposed by Brial et al. [30], this expansion is due to the generation of gases from hydro reactivity reactions. The last traces of hydro reactivity from the SPL reacted through favorable R^3 test conditions such as a finer particle size, higher pH and higher temperature than the leaching step of the LCL&L process. Since hydro reactivity reactions are very exothermic, even small amounts of hydroreactive materials can generate enough

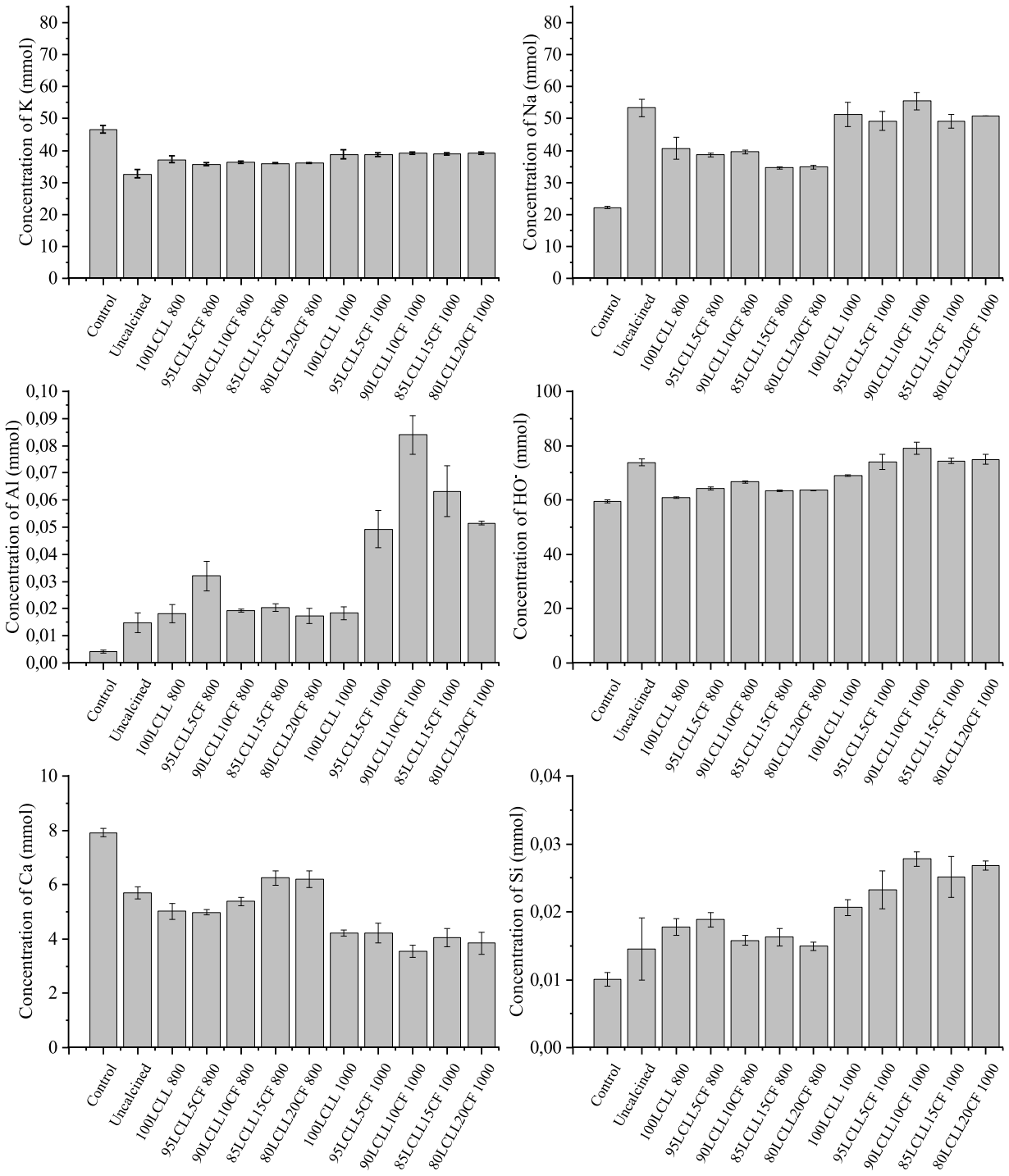

Fig. 7. Concentration in the Frattini solution measured by ICP–OES.

heat to falsify test the R^3 results [30]. However, according to previous studies [19,30], this expansion was not observed for the mixtures of calcined LCLL Ash, which indicates that the heat released is solely due to the reaction of the tested material. These differences of SCM performance between Frattini and R^3 tests had already been described in the literature [33,34,42], which confirms the necessity to not use only one type of test to characterize a new SCM for the first time.

For the LCLL Ash calcined at 800°C, a release of heat of approximately 175 J/g was measured. In addition, for the LCLL Ash/CF calcined at 800°C, similar trends to the Frattini test are observed, such as a decrease in the heat released as the addition of CF increases, particularly for the mixtures with 15% and 20% CF.

The LCLL Ash calcined at 1000°C exhibited a heat released of approximately 225 J/g of SCM. This result is slightly superior to those of LCLL Ash calcined at 800°C, reflecting an increase in reactivity. Unlike the Frattini tests, a trend similar to the mortar results is observable with the addition of CF. The heat release increases for the 5% and 10% additions of CF, which reach approximately 275 and 325 J/g of SCM, respectively. Beyond 10%, the quantity of heat released decreases, reaching approximately 300 J/g of SCM with the mixes containing 15% and 20% CF.

On the same samples, the consumption of portlandite was also measured to confirm the pozzolanic behavior observed during the Frattini tests. The portlandite consumption results are shown in Fig. 8b.

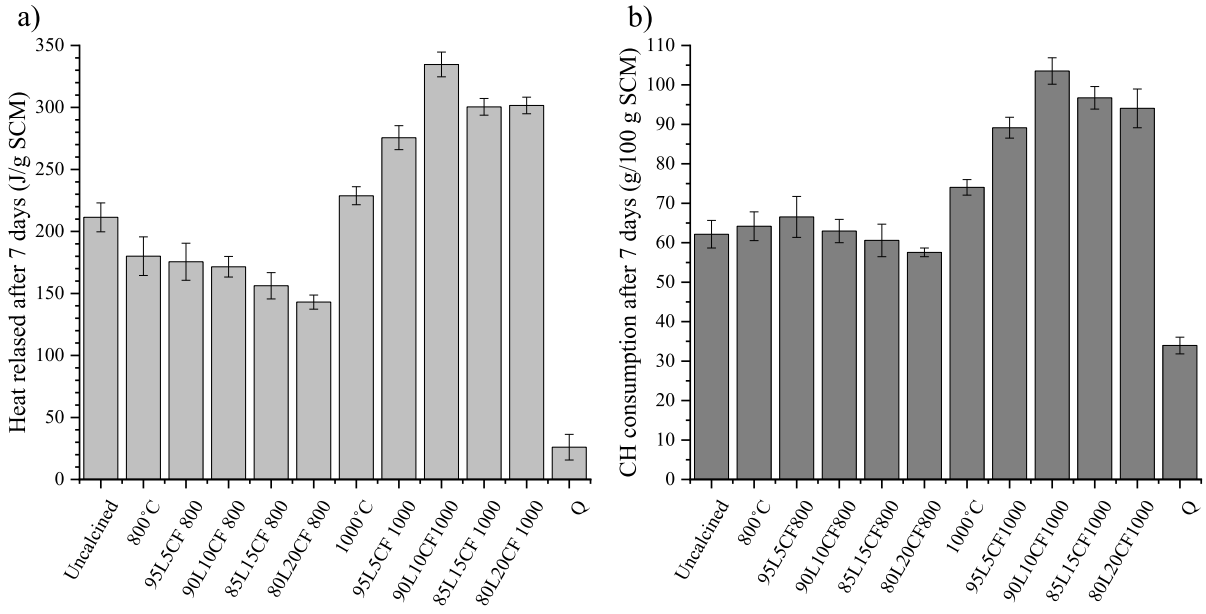

Fig. 8. (a) Heat release and (b) calcium hydroxide consumption after 7 days at 40°C.

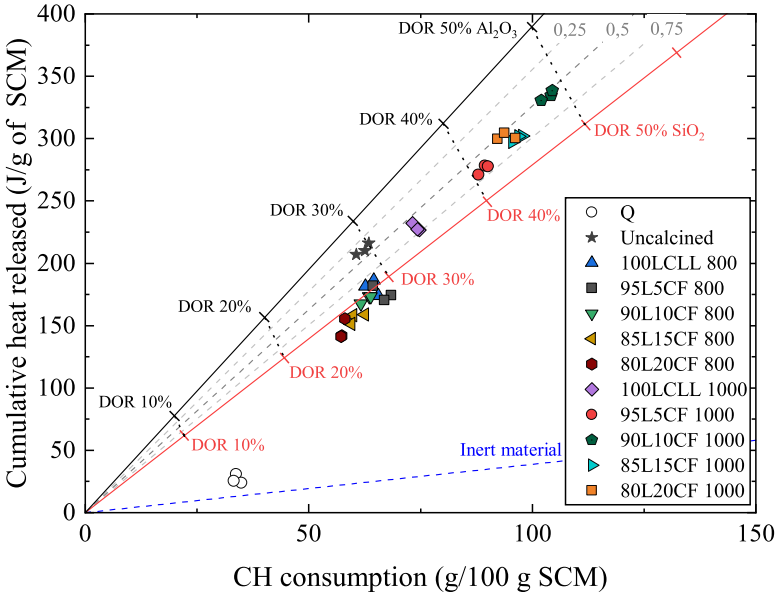

Fig. 9. R^3 test heat released as a function of portlandite consumption for the calcination temperatures studied for the different degree of reaction (DOR) from the thermodynamics simulations.

Unlike the Frattini test, the quartz powder showed a consumption of portlandite of approximately 30 g/100 g of SCM. This low consumption is due to the higher quartz solubility under the conditions of the R^3 test at 40°C. Similar quartz behavior was observed by Li et al. and Suraneni et al. [42,49]. For the release of heat, the noncalcined LCLL Ash also showed a significant consumption of portlandite, at approximately 62 g/100 g of SCM. However, hydro reactivity reactions release aluminum ions that can lead to hydrated phase precipitation, causing portlandite consumption and heat generation [10]. For the LCLL Ash calcined at 800°C, a consumption of portlandite of approximately 65 g/100 g of SCM was observed. The addition of 5% CF will slightly increase the portlandite consumption; however, for CF additions above 10%, a gradual decrease in portlandite consumption was observed, which reflects a slight decrease in reactivity.

The LCLL Ash calcined at 1000°C showed an increase in portlandite consumption compared to the mix calcined at 800°C, which confirms the increase in reactivity with the calcination temperature. The increase in portlandite consumption at 1000°C with the addition of CF was observed until a replacement of 10% CF was reached. These results are consistent with the observations made regarding the mortars and the Frattini tests.

As shown by Suraneni et al. [49], it is possible to plot the heat released versus the consumption of portlandite to classify the SCMs reactivity. Additionally, results of thermodynamic simulations performed by Brial et al. on the R^3 system with GEMS-PSI [19]. These simulations study three different systems to represent an SCM composed of 100% reactive silica, 100% reactive alumina and a totally inert SCM. From these curves, it is possible to predict the reactive silica/reactive alumina ratio for the tested pozzolanic materials. The blue dotted line represents the third system with an inert material. The inert behavior of

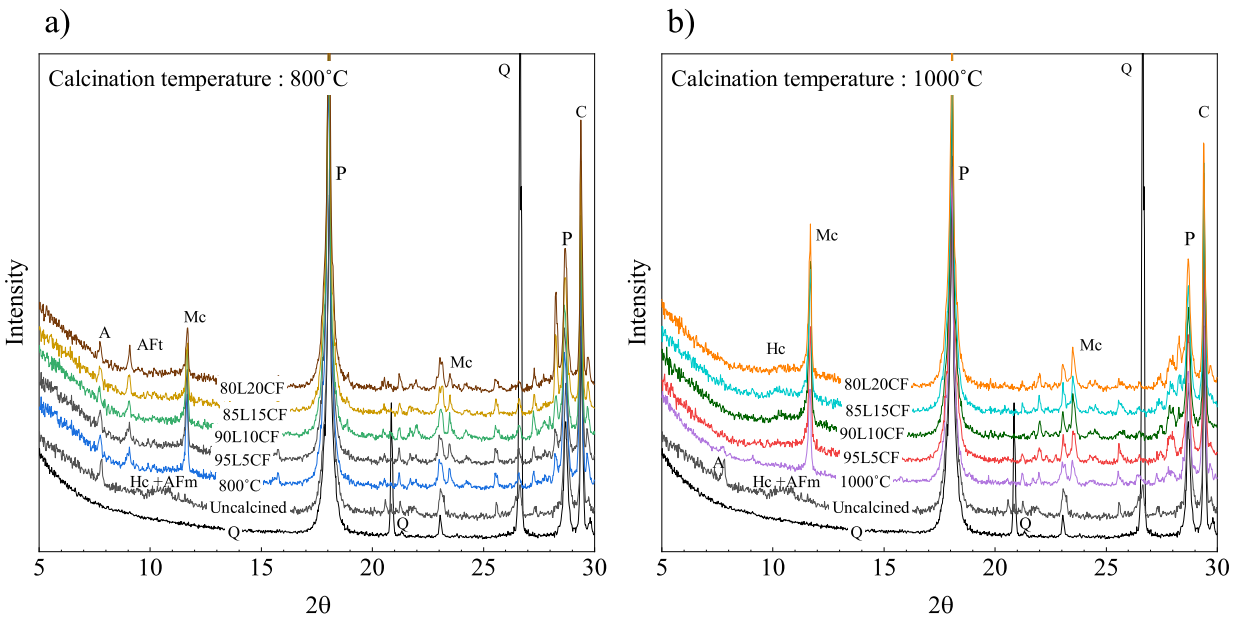

Fig. 10. R^3 mixes XRD spectra. (P: Porlandite, Q: quartz, AFt: ettringite, Mc: monocarboaluminate, Hc: hemicarboaluminate; A: Na-β alumina).

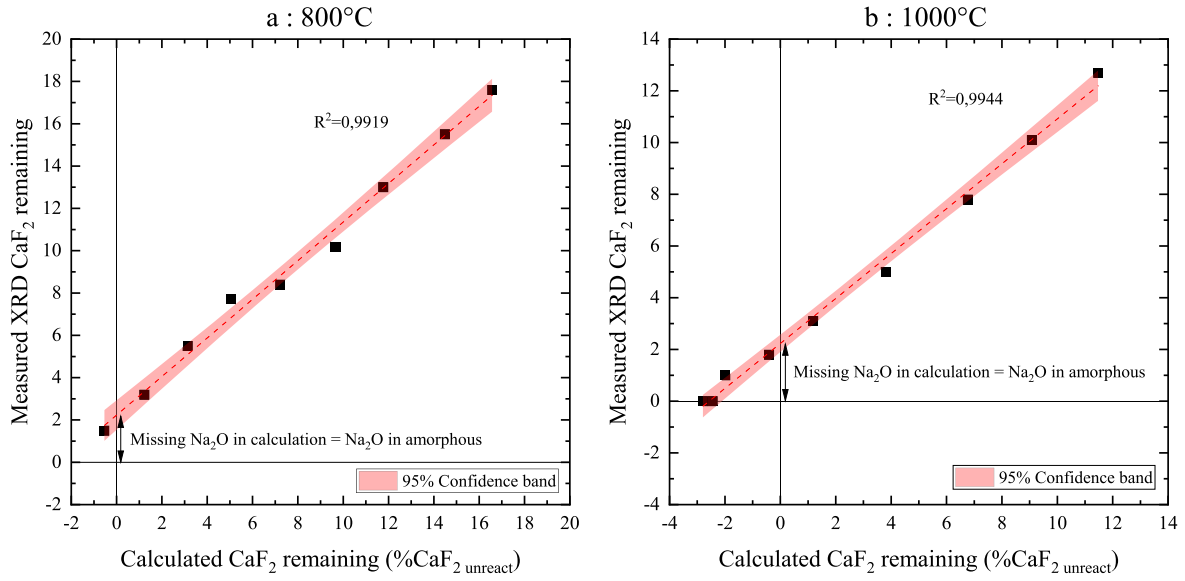

Fig. 11. Amorphous oxide compositions calculated from quantitative XRD as a function of CF addition at a) 800°C and b) 1000°C.

the quartz powder is then clearly identifiable, showing low heat release and average portlandite consumption. The results of the R^3 test heat released as a function of portlandite consumption are presented Fig. 9. The uncalcined LCLL Ash appears to show pozzolanic reactivity. However, as explained above, these results are mainly due to the hydro reactivity phenomenon of LCLL Ash under R^3 conditions as alreadyobserved by Brial et al. [19]. In addition, a comparison of uncalcined LCLL-Ash with thermodynamic models seems to indicate a reactive silica/alumina ratio of approximately 30%/70%. This ratio is higher than the oxide composition of LCLL Ash, which confirms the release of aluminum ions in solution with hydro reactivity reactions.

All of the calcined LCLL Ash/CF showed pozzolanic behavior. However, a slight decrease in the reactivity is observable with the increase in the CF addition for the mixtures calcined at 800°C. Moreover, these mixtures showed results slightly lower than the curve of the thermodynamic model of silica, which indicates that the reactive part is rich in silica. For the mixtures calcined at 1000°C, variable levels of reactivity depending on the concentration of CF were observed. The LCLL Ash calcined without the addition of CF shows the weakest reactivity but remains higher than the LCLL Ash calcined at 800°C. In addition, a lower silica aluminum ratio is also observed, which indicates the presence of a greater amount of reactive aluminum. Additionally, this ratio is similar to the oxide composition of LCLL Ash. With the addition of CF, the reactivity will gradually increase while remaining in the pozzolanic region and reaches a maximum with 10% CF. The reactive silica/alumina ratio will also increase to approximately 50%/50%, which indicates the ever-increasing presence of reactive alumina. However, increasing the addition of CF to 15 to 20% replacement will then slightly decrease the reactivity while keeping the silica/alumina ratio close to 50%/50%.

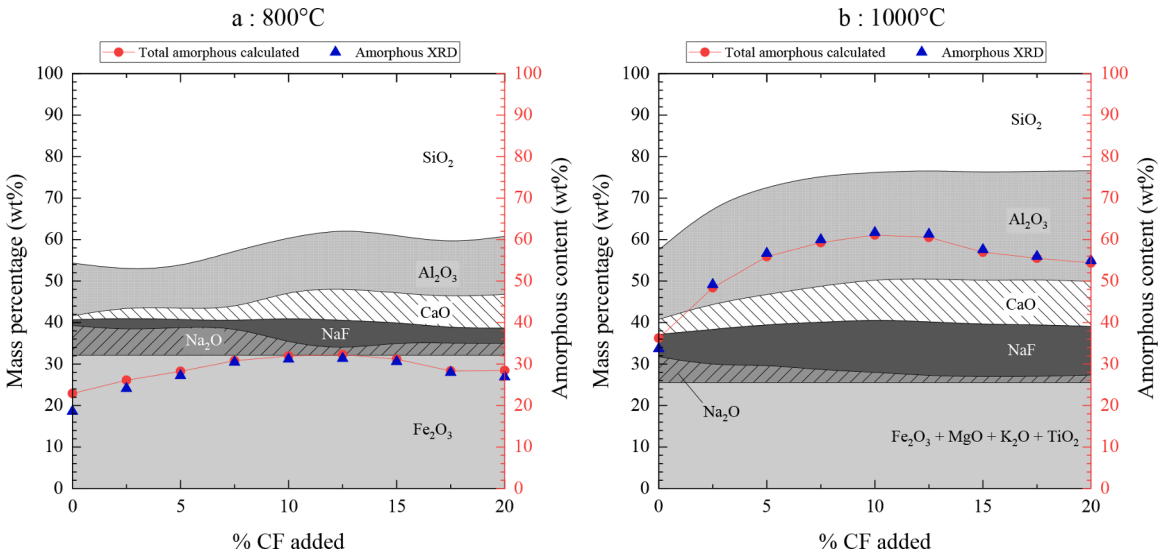

Fig. 12. Amorphous oxide compositions calculated from quantitative XRD as a function of CF addition at a) 800°C and b) 1000°C.

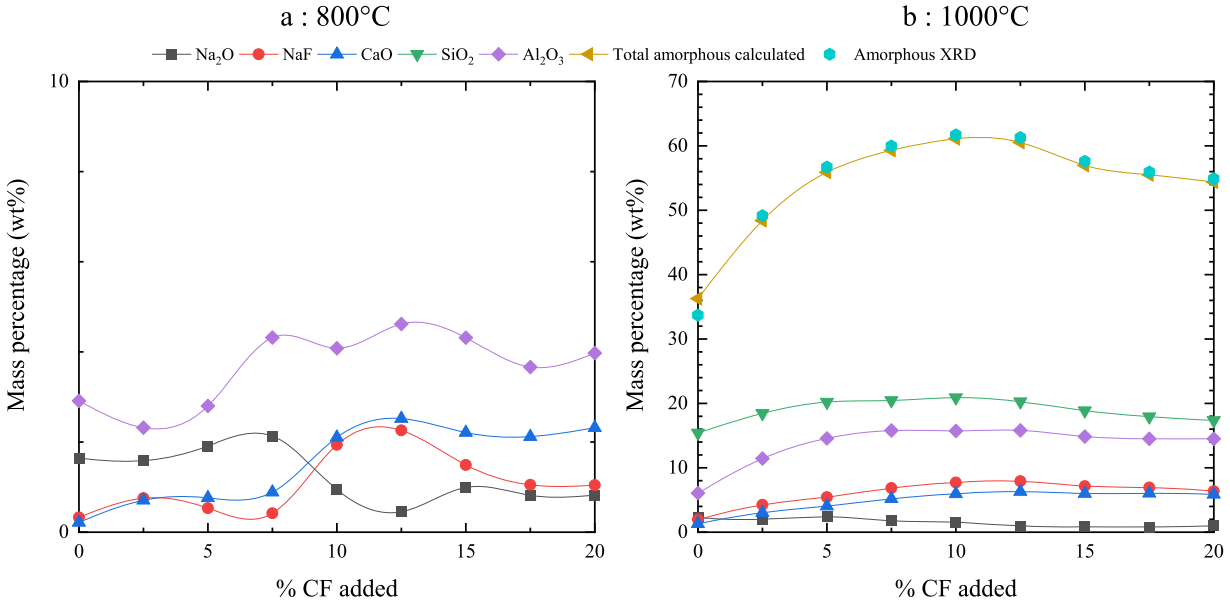

Fig. A1. Amorphous oxide composition calculated from XRD data a) at 800°C and b) at 1000°C.

R3: X-ray diffraction

The diffractograms acquired by XRD on the R^3 samples extracted from the calorimetry ampoules are presented Fig. 10a and b. The quartz powder reference showed a peak for the major phases contained in R^3 paste with portlandite at 18° 2θ (calcium hydroxide), calcite at 29.4° 2θ and quartz at 26.6° 2θ. For uncalcined LCLL Ash, peaks of monosulfoaluminate (AFm) and hemicarboaluminate (Hc) phases were observed at 10.3° 2θ and 10.8° 2θ, respectively [50–52]. These phases indicate the presence of reactive alumina in LCLL Ash in the majority released by the hydro reactivity reaction. As shown in Fig. 10a, both the calcined LCLL Ash and LCLL Ash/CF at 800°C show the formation of ettringite (AFt) with a peak at 9° 2θ and monocarboaluminate (Mc) with a peak at 11.7° 2θ [52,53]. This trend remains observable for all CF additions from 5% to 20%. The addition of fluorite does not seem to affect the precipitation of new phases.

Fig. 10b presents the diffractograms for both calcined LCLL Ash and LCLL Ash/CF at 1000°C. Unlike mixtures calcined at 800°C, the presence of AFt is no longer visible. However, an increase in the intensity of the peak of Mc was observed, which indicates a greater concentration of Mc. Moreover, with the increase in the addition of CF, a peak of Hc is visible at 10.3° 2θ. The presence of Hc seems to indicate a greater quantity of available aluminum and a decrease in the CO_2/Al_2O_3 ratio [54]. For each diffractogram, the crystalline composition of the R^3 hydrated paste was analyzed by Rietveld analysis with an external standard. The quartz reference shows a slight decrease in portlandite and a small amount of amorphous material. In addition, the crystalline quantity of quartz is estimated to be approximately 21 g/100 g against the 22.2 g/100 g initially mixed in the R^3 paste. These results confirm the low reactivity of quartz under the conditions of the R^3 test, allowing a small quantity of C-S-H to precipitate. For the uncalcined LCLL Ash, a decrease in the amount of portlandite was observed. This decrease is mainly attributable to the precipitation of 2.6 g/100 g hemi-carboaluminate and 3.5 g/100 g AFm due to the presence of aluminum resulting from hydro reactivity reactions. The presence of amorphous minerals is more important than for the quartz powder with 13.5 g/100 g. However, the

amount of amorphous material to be measured also considers the unreacted part of the amorphous or unmeasured SCM. There were a large number of phases present in the LCLL Ash, and not all of them could be identified and quantified.

For the different percentages of CF added, the LCLL Ash/CF calcined at 800°C shows a composition similar to that of the calcined LCLL Ash. The LCLL Ash calcined at 1000°C shows a lower ettringite concentration of 0.6 g/100 g and a strong increase in the amount of monocarboaluminate of 9.8 g/100 g. A decrease in the calcite concentration was also observed. This decrease is due to the great precipitation of monocarboaluminate. In addition, the increase in the amount of amorphous material to 21.2 g/100 g and the decreased portlandite content indicate the precipitation of new phases such as C-S-H [53]. The addition of CF will lead to an increase in the concentration of monocarboaluminate up to a maximum of 12.6 g/100 g with 10% CF. The precipitation of hemi-carboaluminate will also increase to reach approximately 2.4 g/100 g. Moreover, for the same mixture, the greatest increase in amorphous content is also observed, with a value of 24 g/100 g. Beyond 10% CF, the concentrations of monocarboaluminate, hemi-carboaluminate, and amorphous decreased to reach values similar to those in LCLL Ash without the addition of CF.

Discussion

Effect of CF addition on LCLL Ash calcination

At high-temperature calcination, the reactions of LCLL Ash can be described according to the SiO_2-Al_2O_3-Na_2O system. Without calcination, the main phases are nepheline, corundum, quartz, albite and β-alumina. Even if these phases only have high melting points, the presence of a eutectic in the nepheline/albite system allows the creation of amorphous materials at lower temperatures [55,56]. With calcination at 800°C, quartz and β-alumina are less stable. These phases will react with each other to form some of the amorphous phase and with corundum to form more nepheline. Increasing the calcination temperature to 1000°C allows the generation of more amorphous phases mainly by the reaction between quartz and β-alumina but also by the fusion of phases such as nepheline. However, the formation of albite or anorthite has also been observed, which limits the amorphous phase concentration. The addition of CF increases the calcium concentration within the LCLL Ash/CF mix, which changes the chemical equilibria according to the temperature. However, the incorporation of calcium into the calcined LCLL Ash leads to the following reaction between sodium and fluorite according to Eq. 6:

$$CaF_2 + Na_2O = 2\,NaF + CaO \quad (6)$$

From the quantitative XRD results, it is possible to calculate the amount of Na_2O present in the crystalline phases according to Eq. A.3. By comparing this value to the total amount in the LCLL Ash/CF mixture, it is possible to deduce the amount of missing Na_2O. Assuming that all of the missing Na_2O has reacted with the fluorite, it is possible to calculate the residual fluorite and compare it to the XRD results. The calculation method is presented in the appendix. As shown in Fig. 11a and b, the quantities of fluorite calculated according to Eq. A1 are strongly correlated with the values measured by XRD.

These results show the importance of sodium in the reactions between LCLL Ash and fluorite. However, an intercept different from 0 indicates that all of the Na_2O did not react with the fluorite and is, therefore, found in the amorphous state. It is therefore always possible to calculate the oxide composition of the amorphous phase from XRD data according to Eqs. A.2 to A.6. Fig. 12a and b show the calculated oxide proportions of the amorphous part as a function of the addition of CF for calcination temperatures of 800°C and 1000°C, respectively.

Two systems are observable. At 800°C, the reaction between the quartz and part of the β-alumina will allow the formation of approximately 20% amorphous phase, which is mainly rich in silica. However, approximately 80% of the Na_2O mass is taken up by the formation of nepheline, which is more stable at that temperature [36]. As Na_2O becomes less available, the reaction between Na_2O and fluorite becomes weaker, and less CaO is produced. The low concentration of CaO and the temperature of 800°C therefore limit the formation of anorthite [57]. However, the excess fluorite will force the reaction of the remaining Na_2O to generate NaF and CaO, which will remain in the amorphous phase. This allows a better incorporation of aluminum into the amorphous phase and increases the amorphous phase concentration. When the CF content is above 12.5%,the Na_2O concentration decreases, limiting the formation of CaO, and the incorporation of aluminum in the amorphous phase.

At 1000°C, the destabilization of nepheline causes the generation of more sodium, silica and alumina in the amorphous phase. The higher concentration of Na_2O promotes the reaction with fluorite and allows more CaO to be produced. At this temperature, part of the calcium will then react with the nepheline and allow the formation of anorthite, which is more stable at 1000°C [39,40,57,38]. However, for the mixtures calcined at 800°C, mixes containing over 12.5% CF dilute the LCLL Ash, leading to a reduction in the quantity of sodium available, as it was entirely transformed into NaF. This limits the CaO supply and allows an increase in the amount of nepheline or albite, as shown in Fig. 3.

Effect of CF addition on the calcined LCLL Ash reactivity

Changes in the mineralogical composition of calcined LCLL Ash/CF caused by the addition of CF will affect the reactivity. The first impact on reactivity stems from the availability of CF influencing the amorphous content through the reaction between fluorite and Na_2O. At 800°C, most of the Na_2O is present as nepheline; however, nepheline, albite and anorthite have solubilities similar to quartz when present in a basic medium [29,58,59], which limits the reactivity of the LCLL Ash. Analysis of the Frattini's test solution shows that the formation of nepheline reduces the amount of rapidly soluble alkalis. Given the high alkali concentration of LCLL Ash, capturing sodium in a less soluble phase could be interesting to limit the risks of alkali-aggregate reactions [3]. The addition of CF slightly increases the quantity of amorphous material by allowing a better incorporation of aluminum and calcium. Moreover, the amorphous part is mainly rich in silica, which promotes pozzolanic-type reactions to precipitate C-S-H. However, as shown by XRD tests on R^3 pastes, some of the aluminum will also react to form ettringite or monocarboaluminate [54]. Increasing the addition of CF to the calcined LCLL Ash at 800°C entails a decrease on the reactivity of the calcined LCLL Ash/CF mixture. A decrease from 30% to 25% in the degree of reaction is observed in Fig. 9, with the increase of CF addition. These changes are explained by a reduced quantity of silica and aluminum available. Similar results are observed for the mortar tests, Frattini tests and R^3 tests.

At 1000°C, the highest proportion of Na_2O available increases the amount of amorphous material by enhancing the incorporation of aluminum and calcium. However, for CF additions above 12.5%, the amount of Na_2O available is limited, which decreases the amorphous content. This explains why the optimum amorphous content is created between 10% and 12.5% CF addition. In this case, the reactivity of the calcined LCLL/CF mixture is proportional to the quantity of amorphous material, which further explains why the mixture with 10% CF is the most reactive. In addition, the higher sodium concentration of the amorphous part causes an increase in the concentration of alkalis in the solution and an increased pH. This increase in pH will also promote the solubility of the amorphous part and increase the reactivity as shown in Fig. 9. The increase in pH and the larger proportion of reactive aluminum shown in Fig. 13b favor the precipitation of monocarboaluminate [60]. Moreover, unlike mixes calcined at 800°C, ettringite did not precipitate due to its lower stability in presence of a higher pH and higher CO_3/SO_4 ratio environment in the R^3 paste [54]. The high concentration of aluminum available with LCLL Ash/CF

calcined at 1000°C makes these mixtures a good candidate for the production of LC^3-type mixtures [26]. These blended cements composed of 50% clinker can be considered as an alternative to reduce the environmental and energetic impacts without affecting the binder performance [27]. Even if the calcination of LCLL Ash/CF requires reaching 1000°C, this temperature remains lower than the clinkerization temperature of Portland cement. In addition, the absence of calcite in the LCLL Ash/CF mixture would further reduce the carbon impact of blended cements containing calcined LCLL Ash/CF. Finally, in Quebec, a province without local clay rich in kaolin, the use of calcined LCLL Ash/CF would allow the production of LC^3 mixtures with local materials and further promote the circular economy between the aluminum and cement industries.

Conclusion

The following concluding remarks can be drawn from the results found in this paper.

a) The valorization of treated SPL and fluorite byproducts from the LCLL process in cementitious materials could be an interesting alternative to conventional SCMs to decrease the environmental footprint of the aluminum and cement industries. It decreases the environmental impacts of their materials by reusing local industrial by-products and avoiding the economic cost of the use of landfills.
b) The composition of the calcined LCLL Ash/CF mix depends on the reaction between fluorite and Na2O. At 800°C, the majority of sodium is present as nepheline, which limits the generation of the amorphous phase; however, at 1000°C, the destabilization of nepheline allows an increase in the availability of sodium, which then reacts with fluorite to generate increased levels of amorphous materials and anorthite. At both calcination temperatures, an optimal amorphous content is observed with CF replacements between 10% and 12.5%.
c) The reactivity of calcined LCLL Ash/CF mainly depends on the quantity of amorphous material. At 800°C, the slight amorphous increase causes little change in the reactivity of the LCLL Ash. However, the important concentration of nepheline allows the capture of more alkalis. However, at 1000°C, the high amorphous content created enhances the reactivity of the LCLL Ash by increasing the formation of CSH and precipitating monocarboaluminate.
d) An optimal mix was found, which was an addition of 10% CF to LCLL Ash calcined at 1000°C. The calcination temperature is lower than the cement clinker production temperature, which reduces the energy consumption of the production.

Declaration of Competing Interest

The authors declare that they have no known competing financial interests or personal relationships that could have appeared to influence the work reported in this paper.

Data availability

Data will be made available on request.

Acknowledgments

The authors are grateful to the NSERC CRD grant program (CRDPJ 515485–17), CRITM consortium, Rio Tinto and Ciment Québec Inc. for their financial support of this project.

Appendix A

Assuming that all of the Na_2O available in the amorphous phase has reacted according to the following equation:

$$CaF_2 + Na_2O = 2\,NaF + CaO \tag{7}$$

we can then write the following:

$$\%CaF_{2unreact}(p) = \frac{M_{CaF_2}}{M_{Na_2O}}\left[\%CaF_{2CF}{\cdot}p + (1-p)\,\%CaF_{2LCLL} - \sum_{i=mineral\ phase}(\%Na_2O)_i\,C_{i,\,XRD}(p)\right] \tag{A.1}$$

where $\%CaF_{2CF}$ and $\%CaF_{2LCLL}$ are the percentages of CaF_2 in CF and LCLL Ash, respectively, and p is the proportion of CF added to LCLL Ash. $(\%Na_2O)_i$ is the percentage of sodium oxide in phase i, and $C_{i,\,XRD}(p)$ is the percentage of phase i measured by XRD according to the proportion of CF added to p. M_{CaF_2} and M_{Na_2O} are the molar masses of CaF_2 and Na_2O, respectively.

The percentage in mass of oxide X in the amorphous state is calculated according to Eq. A.2 for X= SiO_2 and Al_2O_3, as follows:

$$\%X_{amorphous}(p) = (1-p)\,\%X_{LCLL} - \%X_{mineral}(p) \tag{A.2}$$

$\%X_{mineral}(p)$ is the total proportion of oxide contained within the mineral part of calcined LCLL Ash/CF at the proportion p of CF.

$$\%X_{mineral}(p) = \sum_{i=phase}(\%X)_i\,C_{i,\,XRD}(p) \tag{A.3}$$

where $(\%X)_i$ is the percentage of oxide X in phase i, and $C_{i,\,XRD}(p)$ is the percentage of phase i measured by XRD according to p, the proportion of CF added.

The Na_2O, NaF and CaO contents in the amorphous phase were calculated according to the following equations:

$$\%Na_2O_{amorphous}(p) = (1-p)\,\%Na_2O_{LCLL} - \%Na_2O_{mineral}(p) - \frac{M_{Na_2O}}{M_{CaF_2}}\left[\%CaF_{2CF}{\cdot}p + (1-p)\,\%CaF_{2LCLL} - C_{CaF_2,\,XRD}(p)\right] \tag{A.4}$$

$$\%NaF_{amorphous}(p) = \frac{2\,M_{NaF}}{M_{CaF_2}}\left[\%CaF_{2CF}{\cdot}p + (1-p)\,\%CaF_{2LCLL} - C_{CaF_2,\,XRD}(p)\right] \tag{A.5}$$

$$\%CaO_{amorphous}(p) = \frac{M_{CaO}}{2M_{NaF}}\%NaF_{amorphous}(p) + \%CaO_{CF}\cdot p \quad (A.6)$$

The results from the equations above are presented according to Fig. A1 below, where a) represents calcination at 800°C and b) represents calcination at 1000°C.

References

[1] P. Friedlingstein, M. O'Sullivan, M.W. Jones, R.M. Andrew, J. Hauck, A. Olsen, G. P. Peters, W. Peters, J. Pongratz, S. Sitch, C. Le Quéré, J.G. Canadell, P. Ciais, R. B. Jackson, S. Alin, L.E.O.C. Aragão, A. Arneth, V. Arora, N.R. Bates, M. Becker, A. Benoit-Cattin, H.C. Bittig, L. Bopp, S. Bultan, N. Chandra, F. Chevallier, L. P. Chini, W. Evans, L. Florentie, P.M. Forster, T. Gasser, M. Gehlen, D. Gilfillan, T. Gkritzalis, L. Gregor, N. Gruber, I. Harris, K. Hartung, V. Haverd, R.A. Houghton, T. Ilyina, A.K. Jain, E. Joetzjer, K. Kadono, E. Kato, V. Kitidis, J.I. Korsbakken, P. Landschützer, N. Lefèvre, A. Lenton, S. Lienert, Z. Liu, D. Lombardozzi, G. Marland, N. Metzl, D.R. Munro, J.E.M.S. Nabel, S.-I. Nakaoka, Y. Niwa, K. O'Brien, T. Ono, P.I. Palmer, D. Pierrot, B. Poulter, L. Resplandy, E. Robertson, C. Rödenbeck, J. Schwinger, R. Séférian, I. Skjelvan, A.J.P. Smith, A.J. Sutton, T. Tanhua, P.P. Tans, H. Tian, B. Tilbrook, G. van der Werf, N. Vuichard, A. P. Walker, R. Wanninkhof, A.J. Watson, D. Willis, A.J. Wiltshire, W. Yuan, X. Yue, S. Zaehle, Global carbon budget 2020, Earth Syst. Sci. Data 12 (2020) 3269–3340, https://doi.org/10.5194/essd-12-3269-2020.

[2] J. Lehne, F. Preston, Making Concrete Change- Innovation in Low-carbon Cement and Concrete, 2018.

[3] P.C. Hewlett, M. Liska, Lea's Chemistry of Cement and Concrete, Elsevier, 2019, https://doi.org/10.1016/C2013-0-19325-7, 5th Edition.

[4] WBCSD, IEA, Cement Technology Roadmap 2009: Carbon emissions reductions up to 2050, (2009) 36. https://doi.org/978-3-940388-47-6.

[5] M. Taylor, C. Tam, D. Gielen, Energy efficiency and CO 2 emissions from the global cement industry, IEA-WBCSD Cement Energy Effic. Indust. Worksh. (2006) 4–5.

[6] UN Environment, K.L. Scrivener, V.M. John, E.M. Gartner, Eco-efficient cements: potential economically viable solutions for a low-CO2 cement-based materials industry, Cem. Concr. Res. 114 (2018) 2–26, https://doi.org/10.1016/j.cemconres.2018.03.015.

[7] C. Strazza, A. Del Borghi, M. Gallo, M. Del Borghi, Resource productivity enhancement as means for promoting cleaner production: Analysis of co-incineration in cement plants through a life cycle approach, J. Clean. Prod. 19 (2011) 1615–1621, https://doi.org/10.1016/j.jclepro.2011.05.014.

[8] Natural Resources Canada, Aluminum Facts, (2019) 1–10. https://www.nrcan.gc.ca/our-natural-resources/minerals-mining/minerals-metals-facts/aluminum-facts/20510#L2.

[9] F.M. Kimmerle, J.-L. Bernier, V.K. Kasireddy, G. Holywell, Chemical Revovery from Spent PotLining, The Minerals, Metals & Materilas Society, 1993, pp. 671–685.

[10] S. Broek, H.A. Øye, Fundamentals of Managing Spent Potlining (SPL), Travaux 46, in: Proceedings of 35th International ICSOBA Conference, 2018, pp. 817–834.

[11] H.A. Øye, Discussion of Industrial Spent Pot Lining Treatment, in: Proceedings of 35th International ICSOBA Conference, Hamburg, Germany, 2017, pp. 2–5.

[12] R.P. Pawlek, SPL: An update. Minerals, Metals and Materials Series, 2018, pp. 671–674, https://doi.org/10.1007/978-3-319-72284-9_86.

[13] G. Holywell, R. Breault, An overview of useful methods to treat, recover, or reclycle Spent Potlining.pdf, the minerals, Metal. Materil. Soc. 65 (2013) 1441–1451.

[14] L. Birry, S. Leclerc, S. Poirier, the Lcl & L Process : a Sustainable Solution for the Treatment and Recycling of Spent Potlining, (2016) 467–472.

[15] P.B. Personnet, Treatment and Reuse of Spent Pot Lining, an Industrial Application in a Cement Kiln. Essential Readings in Light Metals, John Wiley & Sons, Inc., Hoboken, NJ, USA, 1999, pp. 1049–1056, https://doi.org/10.1002/9781118647745.ch141.

[16] V. Gomes, P.Z. Drumond, J.O.P. Neto, A.R. Lira, Co-Processing at Cement Plant of Spent Potlining from the Aluminum Industry, Essential Readings in Light Metals: Electrode Technology for Aluminum Production. 4 (2005) 1057–1063. doi:10.1002/9781118647745.ch142.

[17] M. Al Jawi, C.M. Chow, S. Pujari, M. Pan, T. Kulkarni, M. Mahmoud, H. Akasha, S. Abdulla, *Environmental Benefits of Using Spent Pot Lining (SPL) in Cement Production*, Springer International Publishing, 2020. doi:10.1007/978-3-030-36408-3_172.

[18] P. Nunez, Sustainable spent pot line management guidance, Miner. Metal. Mater. Ser. (2020) 1225–1230, https://doi.org/10.1007/978-3-030-36408-3_168.

[19] V. Brial, H. Tran, L. Sorelli, D. Conciatori, C.M. Ouellet-Plamondon, Evaluation of the reactivity of treated spent pot lining from primary aluminum production as cementitious materials, Resour. Conserv. Recycl. 170 (2021), 105584, https://doi.org/10.1016/j.resconrec.2021.105584.

[20] H. Tran, L. Sorelli, O. Ahmat Hisseine, D. Bouchard, V. Brial, T. Sanchez, D. Conciatori, C. Ouellet-Plamondon, Development of sustainable ultra-high performance concrete recycling aluminum production waste, Constr. Build. Mater. 371 (2023), 130212, https://doi.org/10.1016/j.conbuildmat.2022.130212.

[21] X. Wang, H. Jin, L. Zhu, Y. Xu, R. Liu, Z. Piao, S. Qu, Effect of caf2 on the viscosity and microstructure of CaO-SiO2-Al2O3 based continuous casting mold flux, Metals (Basel) 9 (2019), https://doi.org/10.3390/met9080871.

[22] S. Banijamali, B. Eftekhari Yekta, H.R. Rezaie, V.K. Marghussian, Crystallization and sintering characteristics of CaO-Al2O3-SiO2 glasses in the presence of TiO2, CaF2 and ZrO2, Thermochim. Acta 488 (2009) 60–65, https://doi.org/10.1016/j.tca.2008.12.031.

[23] T. TRIBE, P. KINGSTON, W. CALEY, Rheology and constitution of the CaO-SiO-MgO-CaF system, Can. Metallurg. Q. 36 (1997) 95–101, https://doi.org/10.1016/S0008-4433(96)00043-2.

[24] H. ming Wang, L. li Yang, G. rong Li, X. Zhu, H. Zhu, Y. tao Zhao, Effects of B2O3 and CaF2 on melting temperatures of CaO-SiO2-Fe2O3 system fluxes, J. Iron Steel Res. Int. 20 (2013) 21–24, https://doi.org/10.1016/S1006-706X(13)60106-5.

[25] W.C. Kosmatka, Steven H.; Kerkhoff, Beatrix; and Panarese, Design and Control Design and Control of Concrete Mixtures, 2003.

[26] S. Seraj, R. Cano, R.P. Ferron, M.C.G. Juenger, Calcined Clays for Sustainable Concrete, Springer, Netherlands, Dordrecht, 2015, https://doi.org/10.1007/978-94-017-9939-3.

[27] Y. Cancio Díaz, S. Sánchez Berriel, U. Heierli, A.R. Favier, I.R. Sánchez Machado, K. L. Scrivener, J.F. Martirena Hernández, G. Habert, Limestone calcined clay cement as a low-carbon solution to meet expanding cement demand in emerging economies, Dev. Eng. 2 (2017) 82–91, https://doi.org/10.1016/j.deveng.2017.06.001.

[28] J.P. Hamilton, S.L. Brantley, C.G. Pantano, L.J. Criscenti, J.D. Kubicki, Dissolution of nepheline, jadeite and albite glasses: toward better models for aluminosilicate dissolution, Geochim. Cosmochim. Acta 65 (2001) 3683–3702, https://doi.org/10.1016/S0016-7037(01)00724-4.

[29] F.K. Crundwell, On the mechanism of the dissolution of quartz and silica in aqueous solutions, ACS Omega 2 (2017) 1116–1127, https://doi.org/10.1021/acsomega.7b00019.

[30] V. Brial, H. Tran, L. Sorelli, D. Conciatori, C.M. Ouellet-Plamondon, Improvement of treated spent pot lining reactivity in cementitious material by calcination, Develop. Built Environ. (2022), 100098, https://doi.org/10.1016/j.dibe.2022.100098.

[31] ASTM International, C109/C109M − 16a Standard Test Method for Compressive Strength of Hydraulic Cement Mortars Using 2-in . or [50-mm] Cube Specimens), ASTM Standard Book, 2016, pp. 1–9, https://doi.org/10.1520/C0109.

[32] British Standard Euronorm, EN196: Methods of testing cement. Part 5: pozzolanicity test for pozzolanic cement, 2005.

[33] A. Tironi, M.A. Trezza, A.N. Scian, E.F. Irassar, Assessment of pozzolanic activity of different calcined clays, Cem. Concr. Compos. 37 (2013) 319–327, https://doi.org/10.1016/j.cemconcomp.2013.01.002.

[34] S. Donatello, M. Tyrer, C.R. Cheeseman, Comparison of test methods to assess pozzolanic activity, Cem. Concr. Compos. 32 (2010) 121–127, https://doi.org/10.1016/j.cemconcomp.2009.10.008.

[35] F. Avet, X. Li, M. Ben Haha, S.A. Bernal, S. Bishnoi, Ö. Cizer, M. Cyr, S. Dolenec, P. Durdzinski, J. Haufe, D. Hooton, M.C.G. Juenger, S. Kamali-Bernard, D. Londono-Zuluaga, A.T.M. Marsh, M. Marroccoli, M. Mrak, A. Parashar, C. Patapy, M. Pedersen, J.L. Provis, S. Sabio, S. Schulze, R. Snellings, A. Telesca, M. Thomas, F. Vargas, A. Vollpracht, B. Walkley, F. Winnefeld, G. Ye, S. Zhang, K. Scrivener, Report of RILEM TC 267-TRM phase 2: optimization and testing of the robustness of the R3 reactivity tests for supplementary cementitious materials, Mater. Struct./Materiaux et Construct. 55 (2022), https://doi.org/10.1617/s11527-022-01928-6.

[36] Y. Wang, D. Wang, C. Dong, Y. Yang, The behaviour and reactions of sodium containing minerals in ash melting process, J. Energy Instit. 90 (2017) 167–173, https://doi.org/10.1016/j.joei.2016.02.007.

[37] X.D. Chen, L.X. Kong, J. Bai, Z.Q. Bai, W. Li, Effect of Na2O on mineral transformation of coal ash under high temperature gasification condition, Ranliao Huaxue Xuebao/J. Fuel Chem. Technol. 44 (2016) 263–272, https://doi.org/10.1016/s1872-5813(16)30015-9.

[38] X. Zhang, C. Liu, M. Jiang, Effect of fluorine on melt structure for CaO-SiO2-CaF2 and CaO-Al2O3-CaF2 by molecular dynamics simulations, ISIJ Internat. 60 (2020) 2176–2182, https://doi.org/10.2355/isijinternational.ISIJINT-2020-002.

[39] F.H. Li, J.J. Huang, Y.T. Fang, Y. Wang, Mineral matter transformation of coal ash under gasification atmosphere: a case of Huolinhe lignite, Adv. Mat. Res. 347–353 (2012) 3732–3735, https://doi.org/10.4028/www.scientific.net/AMR.347-353.3732.

[40] X. Wu, Z. Zhang, G. Piao, X. He, Y. Chen, N. Kobayashi, S. Mori, Y. Itaya, Behavior of mineral matters in chinese coal ash melting during char-CO 2/H2O gasification reaction, Energy Fuel. 23 (2009) 2420–2428, https://doi.org/10.1021/ef801002n.

[41] M. Cyr, P. Lawrence, E. Ringot, Mineral admixtures in mortars Quantification of the physical effects of inert materials on short-term hydration, 35 (2005) 719–730. doi:10.1016/j.cemconres.2004.05.030.

[42] X. Li, R. Snellings, M. Antoni, N.M. Alderete, M. Ben Haha, S. Bishnoi, Ö. Cizer, M. Cyr, K. De Weerdt, Y. Dhandapani, J. Duchesne, J. Haufe, D. Hooton, M. Juenger, S. Kamali-Bernard, S. Kramar, M. Marroccoli, A.M. Joseph, A. Parashar, C. Patapy, J.L. Provis, S. Sabio, M. Santhanam, L. Steger, T. Sui, A. Telesca, A. Vollpracht, F. Vargas, B. Walkley, F. Winnefeld, G. Ye, M. Zajac, S. Zhang, K.L. Scrivener, Reactivity tests for supplementary cementitious materials: RILEM TC 267-TRM phase 1, Mater. Struct. 51 (2018) 151, https://doi.org/10.1617/s11527-018-1269-x.

[43] I. Odler, R. Wonnemann, Effect of alkalies on Portland cement hydration, Cem. Concr. Res. 13 (1983) 477–482, https://doi.org/10.1016/0008-8846(83)90005-4.

[44] K. Wesche, Fly Ash in Concrete : Properties and Performance, E & FN SPON, 1991.
[45] D.K. Dutta, D. Bordoloi, P.C. Borthakur, Hydration of Portland cement clinker in the presence of carbonaceous materials, Cem. Concr. Res. 25 (1995) 1095–1102, https://doi.org/10.1016/0008-8846(95)00104-K.
[46] C. Guo, J. Zhu, W. Zhou, Z. Sun, W. Chen, Effect of phosphorus and fluorine on hydration process of tricalcium silicate and tricalcium aluminate, J. Wuhan Univer. Technol.-Mater. Sci. Ed. 27 (2012) 333–336, https://doi.org/10.1007/s11595-012-0462-y.
[47] I. Odler, S. Abdul-Maula, Structure and properties of Portland cement clinker doped with CaF2, J. Am. Ceram. Soc. 63 (1980) 654–659, https://doi.org/10.1111/j.1151-2916.1980.tb09855.x.
[48] F. Avet, R. Snellings, A. Alujas, M. Ben, K. Scrivener, Cement and concrete research development of a new rapid, relevant and reliable (R 3) test method to evaluate the pozzolanic reactivity of calcined kaolinitic clays, Cem. Concr. Res. 85 (2016) 1–11, https://doi.org/10.1016/j.cemconres.2016.02.015.
[49] P. Suraneni, A. Hajibabaee, S. Ramanathan, Y. Wang, J. Weiss, New insights from reactivity testing of supplementary cementitious materials, Cem. Concr. Compos. 103 (2019) 331–338, https://doi.org/10.1016/j.cemconcomp.2019.05.017.
[50] J. Skibsted, R. Snellings, Reactivity of supplementary cementitious materials (SCMs) in cement blends, Cem. Concr. Res. 124 (2019), 105799, https://doi.org/10.1016/j.cemconres.2019.105799.
[51] B. Lothenbach, F. Winnefeld, C. Alder, E. Wieland, P. Lunk, Effect of temperature on the pore solution, microstructure and hydration products of Portland cement pastes, Cem. Concr. Res. 37 (2007) 483–491, https://doi.org/10.1016/j.cemconres.2006.11.016.
[52] R. Snellings, A. Bazzoni, K. Scrivener, The existence of amorphous phase in Portland cements: physical factors affecting Rietveld quantitative phase analysis, Cem. Concr. Res. 59 (2014) 139–146, https://doi.org/10.1016/j.cemconres.2014.03.002.
[53] K. Scrivener, R. Snellings, B. Lothenbach, A practical guide to microstructural analysis of cementitious materials edited, 2016. doi:10.7693/wl20150205.
[54] T. Matschei, B. Lothenbach, F.P. Glasser, The role of calcium carbonate in cement hydration, Cem. Concr. Res. 37 (2007) 551–558, https://doi.org/10.1016/j.cemconres.2006.10.013.
[55] G. Lambotte, P. Chartrand, Thermodynamic modeling of the (Al2O3 + Na 2O), (Al2O3 + Na2O + SiO 2), and (Al2O3 + Na2O + AlF 3 + NaF) systems, J. Chem. Thermodyn. 57 (2013) 306–334, https://doi.org/10.1016/j.jct.2012.09.002.
[56] S.A. Utlak, T.M. Besmann, Thermodynamic assessment of the pseudoternary Na2O–Al2O3–SiO2 system, J. Am. Ceram. Soc. 101 (2018) 928–948, https://doi.org/10.1111/jace.15166.
[57] Z.Y. Merkit, H.Ö. Toplan, N. Toplan, The crystallization kinetics of CaO–Al2O3–SiO2 (CAS) glass–ceramics system produced from pumice and marble dust, J. Therm. Anal. Calorim. 134 (2018) 807–811, https://doi.org/10.1007/s10973-018-7571-6.
[58] G. Yuan, Y. Cao, H.M. Schulz, F. Hao, J. Gluyas, K. Liu, T. Yang, Y. Wang, K. Xi, F. Li, A review of feldspar alteration and its geological significance in sedimentary basins: From shallow aquifers to deep hydrocarbon reservoirs, Earth Sci. Rev. 191 (2019) 114–140, https://doi.org/10.1016/j.earscirev.2019.02.004.
[59] L. Chou, R. Wollast, Steady-state kinetics and dissolution mechanisms of albite, Am. J. Sci. 285 (1985) 963–993, https://doi.org/10.2475/ajs.285.10.963.
[60] B.A. Clark, P.W. Brown, Formation of calcium sulfoaluminate hydrate compounds. Part II, Cem. Concr. Res. 30 (2000) 233–240, https://doi.org/10.1016/S0008-8846(99)00234-3.